JOURNAL OF APPLIED CRYSTALLOGRAPHY

Volume 48 (2015)

Supporting information for article:

Structure and morphology of shape-controlled Pd nanocrystals

Jose Solla-Gullon, Emmanuel Garnier, Juan M. Feliu, Matteo Leoni, Alberto Leonardi and Paolo Scardi

Structure and morphology of shape-controlled Pd nanocrystals

Jose Solla-Gullon[a], Emmanuel Garnier[a], Juan M. Feliu[a], Matteo Leoni[b], Alberto Leonardi[b] and Paolo Scardi[b]*

[a] Institute of Electrochemistry, University of Alicante, Carretera de San Vicente del Raspeig s/n, Alicante, 03690, Spain

[b] Civil, Environmental and Mechanical Engineering, University of Trento, Via Mesiano, 77, Trento, Trento, 38123, Italy

Correspondence email: paolo.scardi@unitn.it

Supplementary materials

TEM, HRTEM images and particle size distributions of the nanocrystals used in this work

The samples were centrifuged twice (9000 rpm, 30 min) and redispersed in ultrapure water (Millipore Milli-Q®). TEM images were then obtained for each batch. Due to the presence of CTAB, we observed well-separated nanocrystals having their faces nearly parallel to the plane of observation. Figure S1 shows a representative TEM image of each batch.

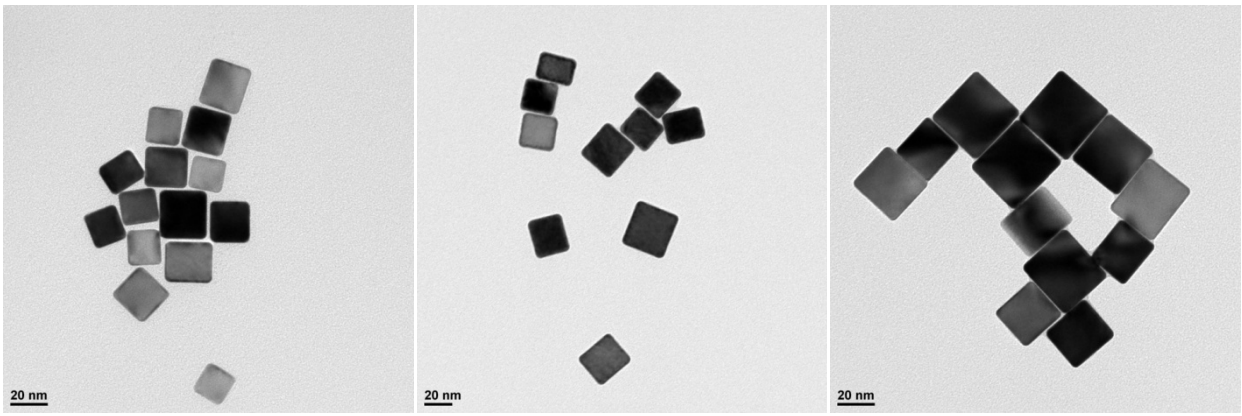

Batch1	Batch2	Batch3

Figure S1. Representative TEM image of each batch

TEM analysis shows that most nanoparticles (93%) have a square or a rectangular footprint. The remaining fraction (7%) is made up mostly of multiply twinned (so-called non crystallographic) nanoparticles like decahedra and icosahedra, but also a few nanorods, flat

triangular prisms (nanosheets), and right bipyramids. Figure S2 shows a representative TEM image containing all these features.

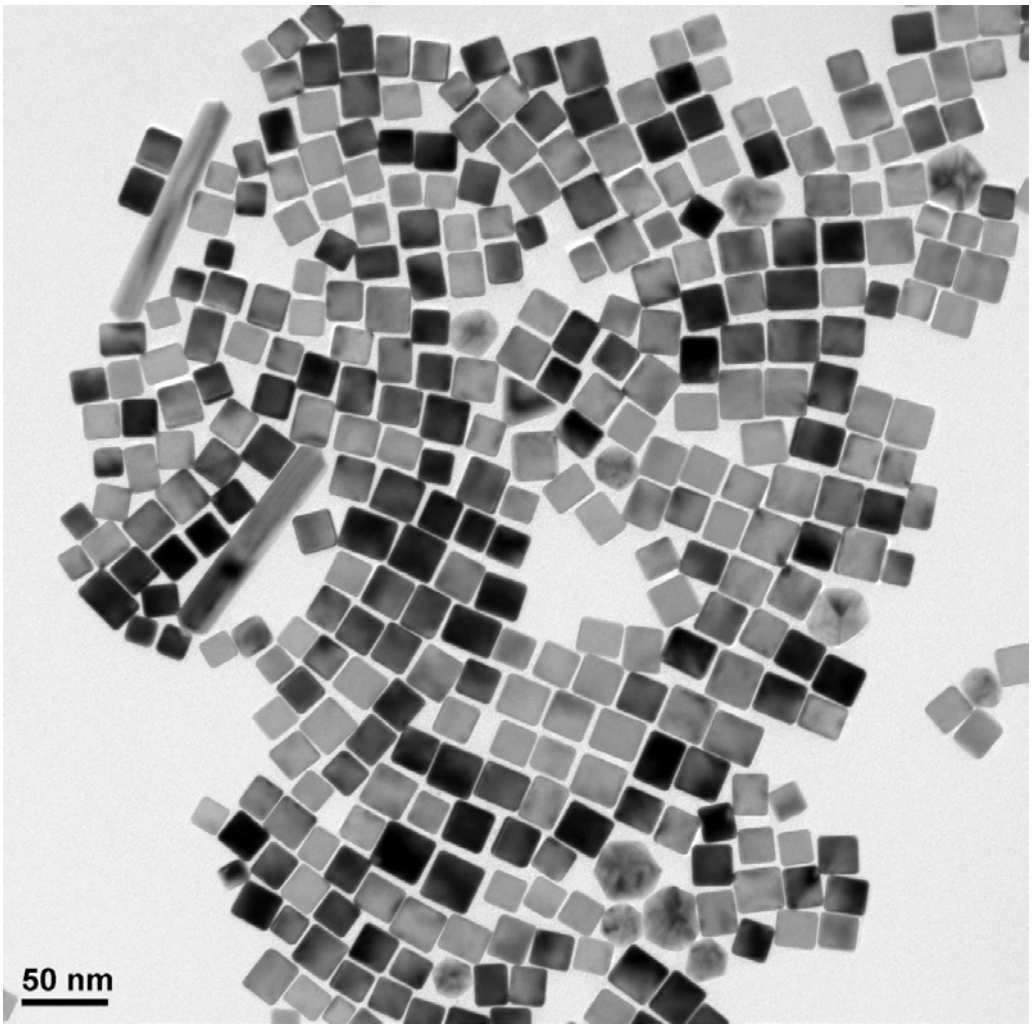

Figure S2. Representative TEM image containing cubes, decahedra, nanorods, flat triangular prisms and right bipyramids.

For the HRTEM experiments, the samples were taken from the NaOH treated aqueous solution (see **specimen preparation** for details). Figure S3 shows a representative HRTEM image of the sample.

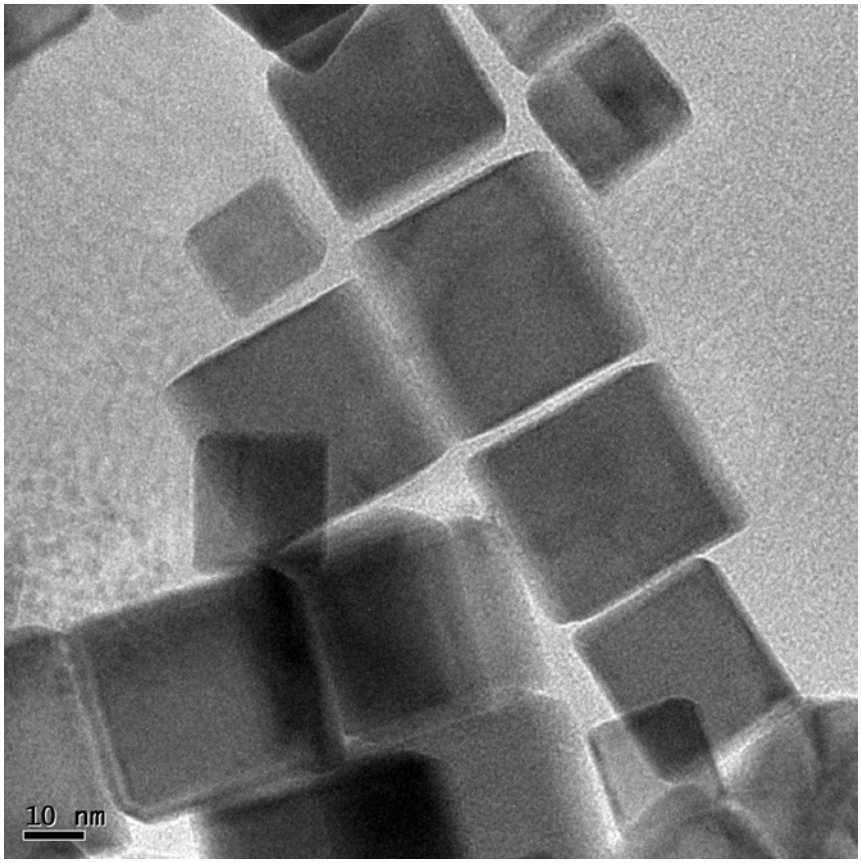

Figure S3. HRTEM image of the sample

A detailed analysis of the HRTEM images shows that the facets are planar, albeit in some cases slightly irregular (Figures S4), while corners and edges are truncated or somehow rounded. The truncations are rounded in most cases (Figures S5a and b) but could be also linear (Figure S5c).

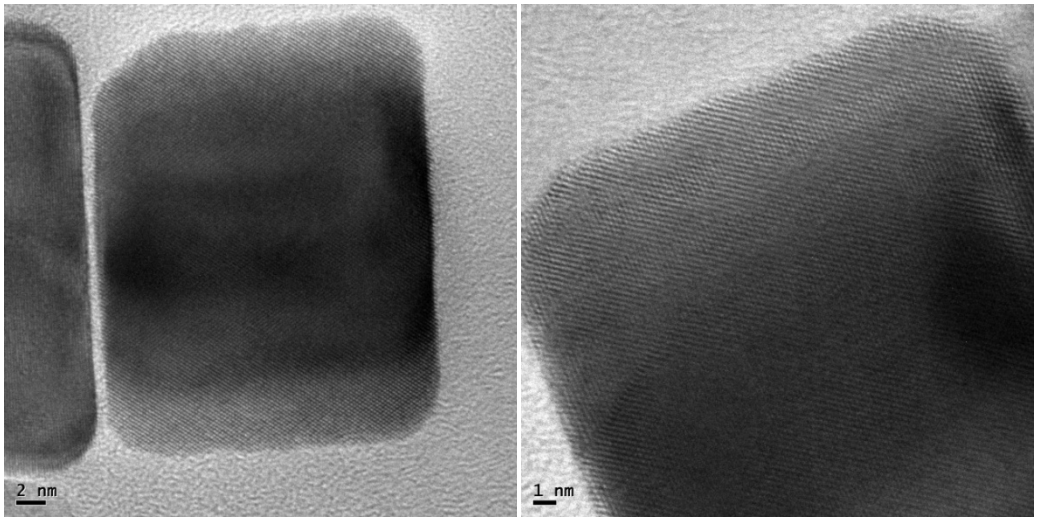

Figure S4. HRTEM images showing {100} facets with steps

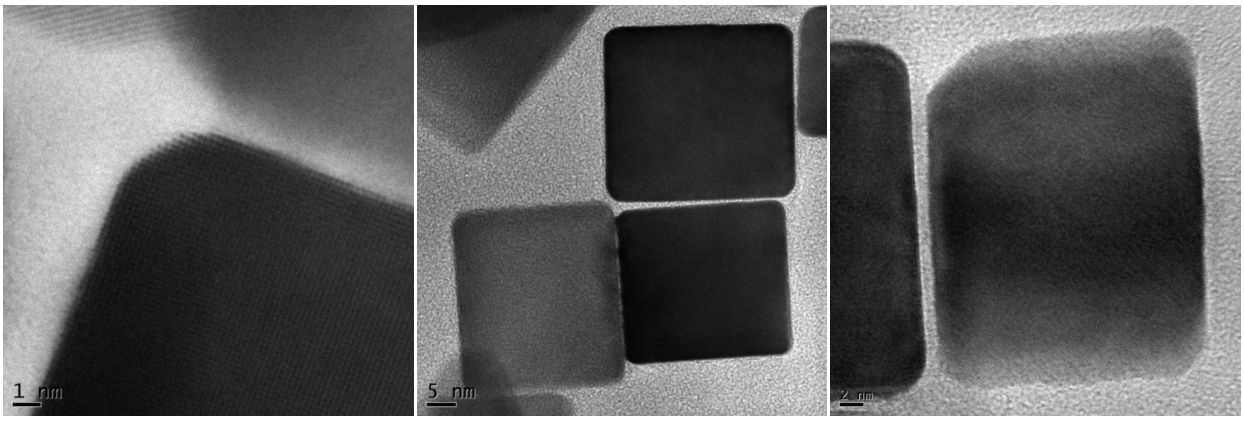

(a)	(b)	(c)

Figure S5. HRTEM images showing rounded truncations (a) and (b) and also linear (c)

Lattice defects are definitely infrequent: stacking faults can be identified in a few nanocrystals, whereas dislocations can only be seen where impacts between nanocrystals have caused plastic deformation (Figure S6)

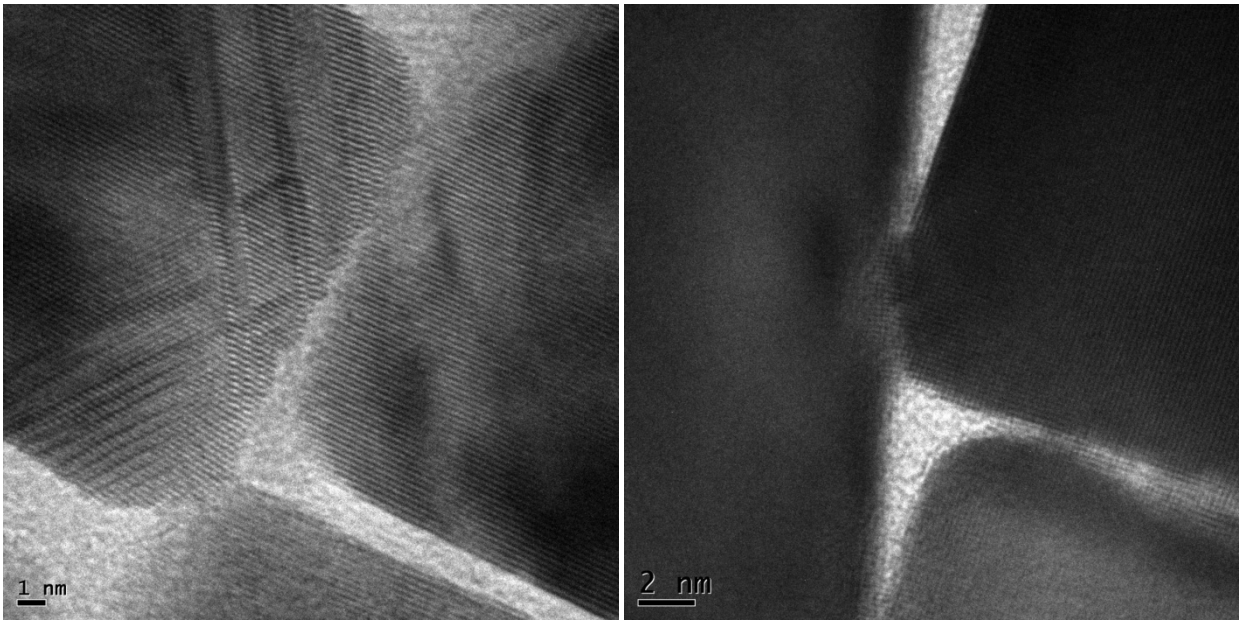

(a)	(b)

Figure S6. HRTEM images showing impact between nanocrystals (a) and plastic deformation (b)

Table 1 Statistics of the different Pd nanocrystal shapes in the three batches produced for this study.

	cubes	nanorods	Triangular nanosheet	Right bipyramids	Icosahedra or decahedra	undefined
Pd batch1	252	1	0	1	14	3
Pd batch 2	1518	5	5	7	84	1
Pd batch 3	464	8	6	3	23	1
Total	2234	14	11	11	121	5
%	93,24	0,58	0,46	0,46	5,05	0,21

Table 2 Particle size statistics of the Pd nanocubes (in nm) in the three batches.

	mean	Stand.dev.	minimum	median	maximum
Pd batch1	24.57	4.04	12.9	24.51	37.89
Pd batch 2	29.06	6.48	12.99	28.57	56.00
Pd batch 3	21.14	2.97	10.32	20.98	30.48
Total distribution	24.92	5.74	10.32	24.06	56.00

XRD results. Diffraction from kapton capillary and absorption correction

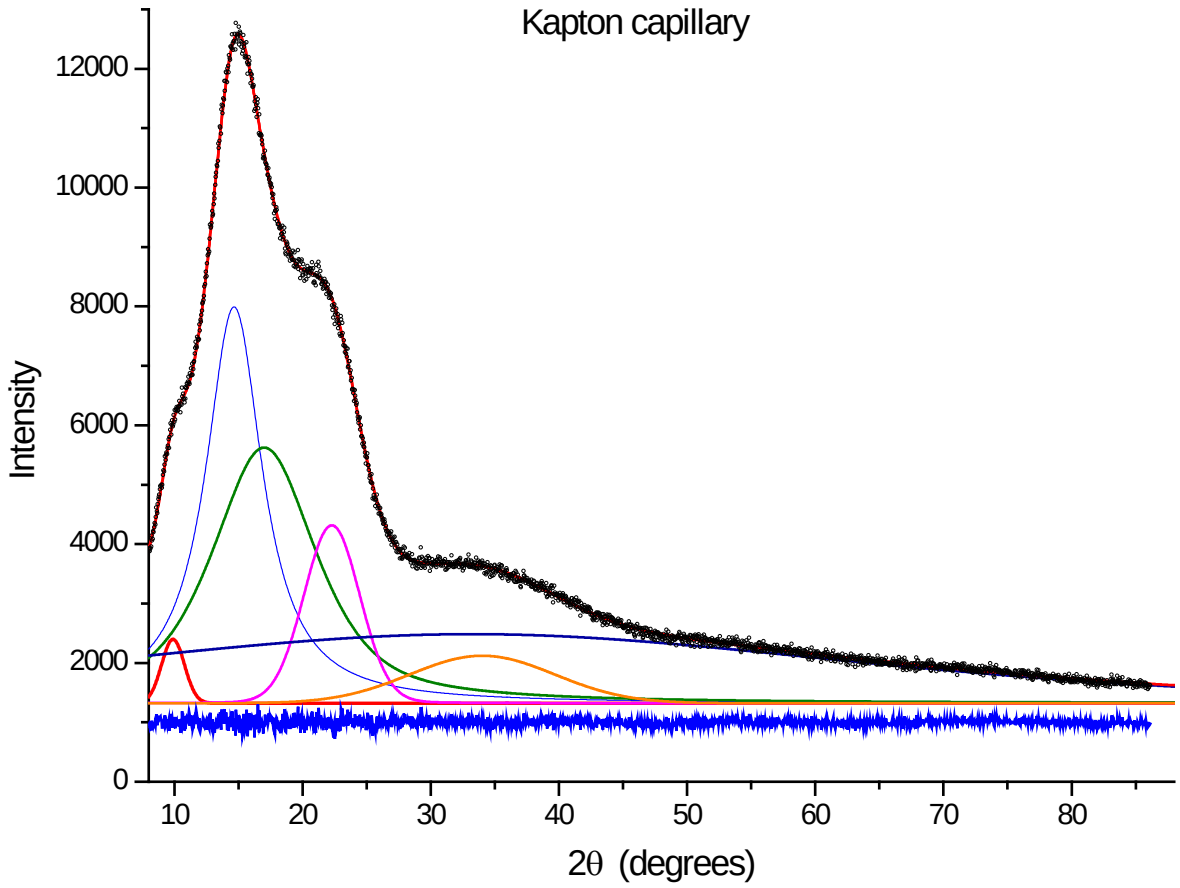

Figure S7. XRD pattern from an empty kapton capillary, measured under the same conditions as the capillary filled with Pd nanoparticles. The figure shows the result of fitting six pseudo-Voigt curves, which were used in parametric form (i.e., scaled by a refinable parameter) to model the background in the WPPM analysis of the Pd nanoparticle data.

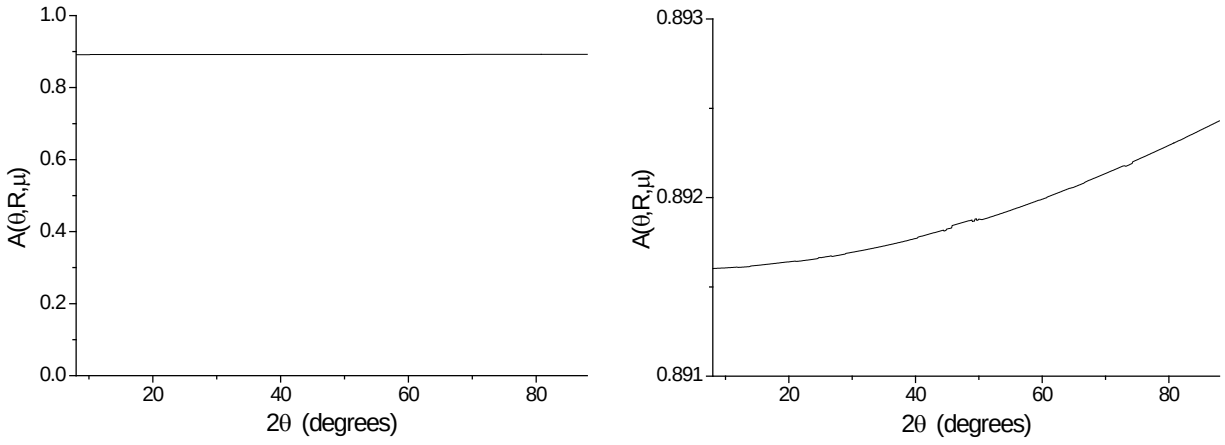

Figure S8. Transmission factor across the measured 2θ range. The trend was calculated from the expression given in the International Tables for Crystallography (Maslen, 2006) for the Debye-Scherrer geometry with capillary radius R = 0.025 cm and absorption coefficient μ = 2.71 cm^{-1}.

Electrochemical characterization

The cubic Pd nanoparticles deposited on glassy carbon were electrochemically characterized in Ar-saturated 0.1 M H_2SO_4 between 0.1 and 0.7 V at 50 mV s^{-1}. Figure S9 shows the voltammetric profiles corresponding to the Pd specimen in 0.1 M H_2SO_4 in which the lower potential is limited to 0.1 V to avoid hydrogen absorption. The voltammetric profiles recorded before and after the CO stripping are similar, indicating that the chemical cleaning of the Pd samples was effective and that the CO adsorption-stripping treatment does not alter their initial surface structure/morphology. Interestingly, the voltammetric profile corresponding to the so-called hydrogen/anion adsorption–desorption region is very similar to that characteristic of a Pd(100) single crystal which, in H_2SO_4, gives sharp anodic and cathodic peaks at about 0.3 and 0.24 V. For the cubic Pd nanoparticles analyzed in this work (Figure S9), these contributions appear at potential values of about 0.30 and 0.23 V, respectively, in good agreement with previous reports for a Pd(100) single crystal (Hoshi et al., 2000; Hoshi et al., 2002; Hoshi et al., 2006; Hoshi et al., 2007; Hara et al., 2007; Kondo et al., 2009).

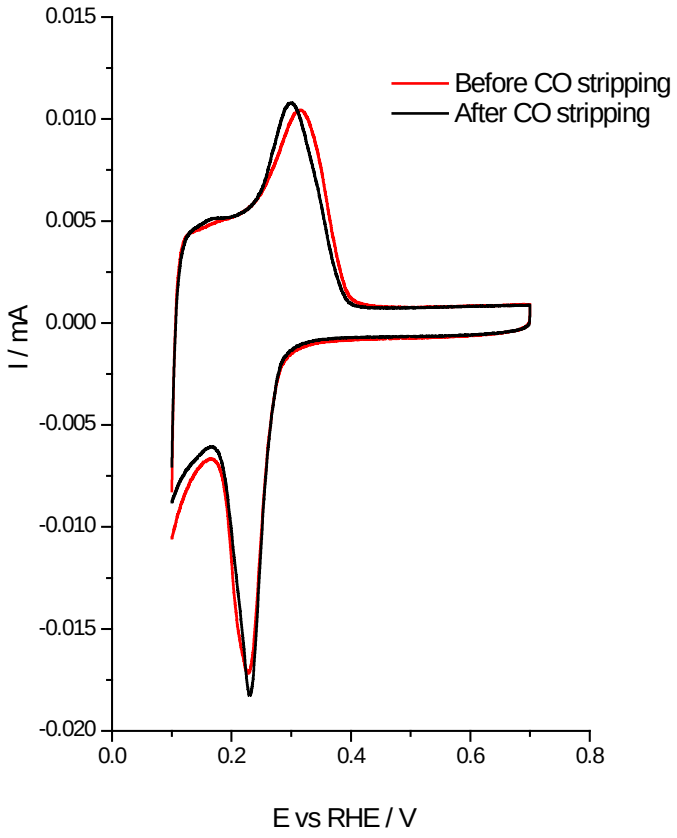

Figure S9. Voltammetric profiles of the cubic Pd nanoparticles before and after the CO stripping cleaning. Test solution 0.1 M H_2SO_4, scan rate 50 mV s^{-1}.

Figure S10 illustrates a typical CO stripping on the Pd nanocubes. A well-defined CO stripping peak is observed at about 0.88 V together with a clear shoulder at about 0.91 V, characteristic signature of a Pd(100) surface structure (Hoshi et al., 2000; Hoshi et al., 2002; Hara et al., 2007). In fact, the intensity of this peak at about 0.91-0.92 V has been correlated to the decrease of the atomic terrace rows on Pd(S)-[n (100) × (110)] and Pd(S)-[n (100) × (111)] electrodes, that is, stepped Pd electrodes with {100} terraces and {110} or {111} surface steps, respectively. Finally, it is worth noting the presence of a cathodic peak at about 0.77 V corresponding to the reduction of Pd surface oxides and whose intensity strongly depends on the upper potential limit (Figure S10).

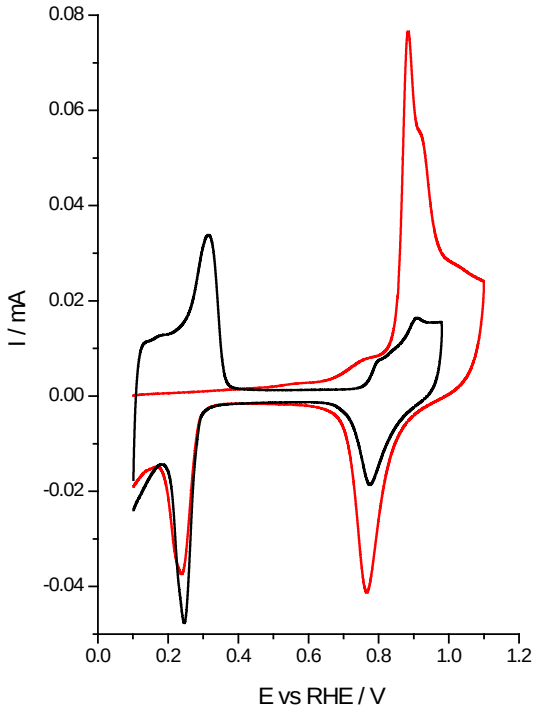

Figure S10. CO stripping and subsequent voltammetric profiles on the Pd nanocubes. Test solution 0.1 M H_2SO_4, scan rate 20 mV s^{-1}.

It is worth noting that from the so-called hydrogen/anion adsorption–desorption region, the active surface area of the Pd sample can be estimated. This surface area calculation is exemplified in Figure S11. The active surface area of the Pd nanoparticles is determined from the area under the so-called hydrogen UPD region (between 0.05 V and 0.6 V) after the subtraction of the double layer charging contribution obtained in 0.1 M H_2SO_4. This area is then transformed into an electric charge (Coulombs) by simply dividing to the scan rate used (0.05 V s^{-1}). Finally, this electric charge is directly converted into active surface area by using a classical charge density value of 212 µC cm^{-2} (Woods, 1976).

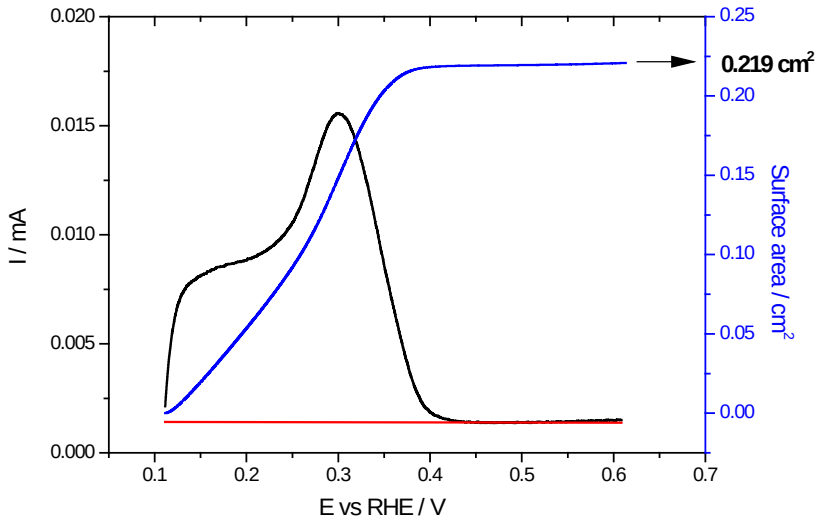

Figure S11. Determination of the electrochemical active surface area from the voltammetric profile of the so-called hydrogen region. Test solution 0.1 M H_2SO_4, scan rate 50 mV s^{-1}.

Cu UPD experiments

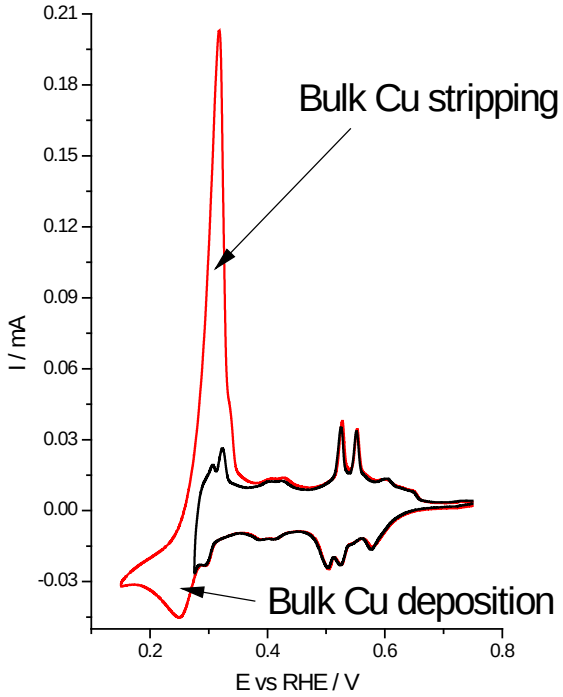

Figure S12. Cu UPD on a polyoriented Pd bead also showing the bulk Cu deposition and stripping. Test solution 0.1 M H_2SO_4 + 1mM $CuSO_4$ + 1mM NaCl, scan rate 50 mV s^{-1}.

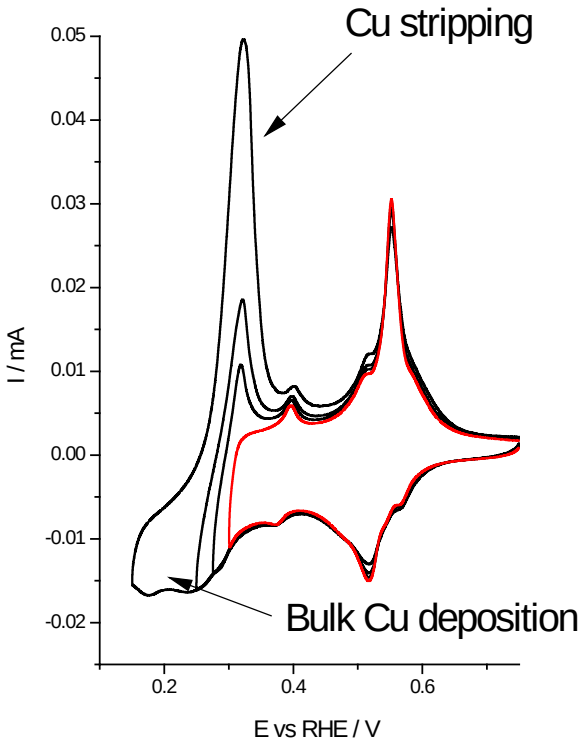

Figure S13. Cu UPD on the Pd nanocubes also showing the bulk Cu deposition and stripping. Test solution 0.1 M H_2SO_4 + 1mM $CuSO_4$ + 1mM NaCl, scan rate 50 mV s^{-1}.

Remarks about the quantification of {100} surface sites on the Pd nanocubes from Cu UPD experiments

As described in the manuscript, to quantify the percentage of {100} surface sites present at the surface of the Pd nanocubes, the Cu UPD voltammetric profile (figure 10) was fitted using five Lorentzian peaks located at the characteristic contributions of the {100}, {110} and {111} surface domains obtained from previous Pd single crystal experiments (Cuesta et al. 1999). The percentage of {100} surface sites is calculated from the area of its corresponding signal respect to the total area of the Cu UPD process. Nevertheless, for a correct calculation, some important points must be taken into account. The first one deals with the nature of the different contributions. Thus, and despite 5 Lorentzian peaks were used, the contribution at about 0.4 V should not be included in the total area of the Cu UPD process because it is accepted to be related to the formation of a second Cu layer on Pd(110) electrodes (Cuesta et al. 1999). Secondly, the area of the different contributions between 0.43 and 0.75 V must be also normalized taking into account the calculated charges for a complete Cu monolayer on Pd(111), Pd(110) and Pd(110) single crystals (486, 421 and 297 µC cm^{-2}, respectively) (Cuesta et al. 1999; Vidal-Iglesias et al. 2006). Consequently, and using the charge for a complete Cu monolayer on a Pd(110) electrode as normalization value, the contributions related to the {111} and {100} must be divided by 1.64 (486/297) and 1.42 (421/297), respectively. Finally, and in order to get a more representative value, as well as to minimize experimental errors,

this analysis was reproduced with different amount of Pd nanocubes. Under these conditions, the percentage of {100} surface sites on the Pd nanocubes was found to be 57 ± 3%.

Additional References

Cuesta, A., Kibler, L., & Kolb, D. (1999). Electroanal. Chem., 466, 165-168.
Hara, M., Linke, U., & Wandlowski, T. (2007). Electrochim. Acta, 52, 5733-5748.
Hoshi, N., Kagaya, K., & Hori, Y. (2000). J. Electroanal. Chem., 485, 55-60.
Hoshi, N., Kida, K., Nakamura, M., Nakada, M., & Osada, K. (2006). J. Phys. Chem. B, 110, 12480- 12484.
Hoshi, N., Kuroda, M., & Hori, Y. (2002). J. Electroanal. Chem., 521, 155-160.
Hoshi, N., Nakamura, M., & Kida, K. (2007). Electrochem. Commun., 9, 279-282.
Kondo, S., Nakamura, M., Maki, N., & Hoshi, N. (2009). J. Phys. Chem. C, 113, 12625-12628.
Maslen, E. N. (2006) International Tables for Crystallography, Wiley, New York, vol. C, chap. 6.3.
Vidal-Iglesias, F., Al-Akl, A., Watson, D., & Attard, G. (2006). Electrochem. Commun., 8, 1147-1150.
Woods, R. (1976) Electroanalytical. Chemistry: a Series of Advances, Marcel Dekker, New York, vol. 9, chap. 1.